# FINAL TECHNICAL REPORT

"Investigation of the Saturn Dust Environment from the Analysis of Energetic Charged Particle Measurements"

L. L. Hood
Lunar and Planetary Laboratory
University of Arizona
Tucson, Arizona 85721
(602) 621-6936

for

J.N. Cuzzi, Chairman
Cassini Dust Environment Workshop
NASA Ames Research Center, 245-3
Moffett Field, California 94035

Period Covered:

January to December 1989

NASA Contract # NAG2-576

## SUMMARY

In order to assist the Cassini project in evaluating risks of collisions with particulate matter in the rotational equatorial plane, available Pioneer 11 and Voyager energetic charged particle data have been reinvestigated to constrain the column mass density of absorbing material within several radial ranges. Within the orbit of Mimas, CRAND proton phase space densities maximize near 2.67 $R_S$ and exhibit a secondary maximum at 2.43 $R_S$. From the condition that sources must exceed losses near these maxima and using available theoretical models for CRAND proton production rates, upper bounds on the column mass density at these two radial locations are calculated to be $2 \times 10^{-8}$ and $9 \times 10^{-8}$ gm/cm$^2$, respectively. Detailed fits of radial diffusion models to the observed flux maxima yield somewhat more restrictive upper limits of $\sim 1 \times 10^{-8}$ gm/cm$^2$ at 2.67 $R_S$ and $\sim 4 \times 10^{-8}$ gm/cm$^2$ at 2.43 $R_S$. These upper limits compare to a lower limit on the column mass density of the G Ring at 2.83 $R_S$ of $\sim 2 \times 10^{-7}$ gm/cm$^2$, estimated from previous model calculations by Van Allen. Aside from continuous rings, longitudinally limited, low-optical depth clouds of particulates may exist in orbit with several of the inner satellites including Mimas and Enceladus. A brief review of Voyager energetic particle microsignatures that suggest the presence of material co-orbiting with these two satellites is presented. Finally, Pioneer 11 and Voyager measurements of low-energy electron fluxes exhibit minima near the location of the tenuous E Ring centered on approximately 4 $R_S$. Pioneer 11 pitch angle distributions appear to support the possibility that direct absorption by Ring E particulates produced the observed flux decreases. Assuming that this is the case, model calculations indicate a column mass density for the E Ring in the range of $5 \times 10^{-11}$ to $5 \times 10^{-10}$ gm/cm$^2$. For an approximate mean normal opacity of $\sim 5 \times 10^{-7}$, estimated from optical data, the corresponding estimated range of E Ring particulate sizes is of order 1 to 10 $\mu$m.


## Introduction

Measurements of energetic charged particles trapped in the Saturnian magnetic field contain information relevant to the existence and sizes of solid particulates in the inner magnetosphere [Thomsen and Van Allen, 1979; Van Allen, 1983]. In addition to constraining models of planetary rings, such information is of practical importance in planning the trajectories of future Saturn orbital missions so as to avoid regions containing sizeable particulates. This report summarizes results from a reinvestigation of relevant energetic charged particle data sets conducted during the past eighteen months in response to a request from the Cassini joint science working group (J.N. Cuzzi, chairman). Most of these results were presented at the final "Cassini Dust Environment Workshop" held January 20, 1989 at JPL. However, parts were also presented at previous workshops held in Pasadena in June 1988 and in November 1987; in addition, a further calculation for the inner CRAND proton zone was carried out after the last workshop in response to comments by workshop members. Although additional calculations may be done over the next few months, the current report presents at least a majority of the pertinent results.

Three primary areas of study were identified as useful for constraining the Cassini orbiter mission design: (1) an evaluation of upper limits on the column mass density of

particulates within relatively clear zones centered on approximately 2.43 $R_S$ (between the F ring and Epimetheus/Janus) and 2.67 $R_S$ (between Epimetheus/Janus and the G ring) using CRAND proton data; (2) a review of satellite microsignature observations relevant to the existence of co-orbiting material, especially near the orbit of Enceladus; and (3) modeling of energetic electron measurements that appear to indicate absorption by E Ring particulates in order to constrain the column mass density and mean particulate size. In the following, relevant data and modeling results are described separately for each identified area.

## 1. CRAND Proton Model Calculations and Interpretation

The innermost part of the Saturnian magnetosphere outside the main rings ($2.3 < L < 4$) is populated principally by very energetic protons ($E >> 10$ MeV) that are produced by cosmic ray albedo neutron decay (CRAND) resulting from cosmic ray interactions with ring material and, to a much lesser extent, with the Saturnian atmosphere [Fillius et al., 1980; Van Allen et al., 1980; Blake et al., 1983; Cooper, 1983]. Because of their short drift and bounce periods, they are sensitive indicators of the existence of absorbing solid material in the form of satellites and/or rings. With its relatively low periapsis (1.4 $R_S$) and equatorial trajectory, Pioneer 11 provided the best available measurements of Saturn CRAND proton fluxes versus radial distance. Shown in Figure 1 is a plot of the phase space density of energetic protons with first invariant $\mu = 8.3 \times 10^3$ MeV/Gauss derived by Van Allen et al. [1980] from measurements with the University of Iowa detector C. The first adiabatic invariant is defined as the perpendicular energy of the particle divided by the local magnetic field strength. The phase space density is the directional flux per unit energy and is, according to Liouville's theorem, the quantity that remains constant during radial diffusion in the absence of sources or sinks of particles [Roederer, 1970; Schulz and Lanzerotti, 1974]. Figure 1 is therefore very diagnostic of the dominance of particle sources or sinks within different radial ranges. Specifically, particle sources strongly dominate sinks at the major peak centered at 2.68 $R_S$ while minima occur in association with inner satellites and rings. Secondary peaks occur at 2.43 and 3.37 $R_S$. From the point of view of Cassini mission planning, it is of particular interest to determine quantitative limits on the column mass density of possible orbiting material near the two inner peaks at 2.43 and 2.68 $R_S$.

### The G Ring

Only one previous study, that of Van Allen [1983], has attempted to estimate the amount and properties of material in any part of the inner zone from a model analysis of CRAND proton data. A second study, that of Cooper [1983], developed a detailed theoretical model for the CRAND proton production process. He showed that reasonable fits to observed counting rates near flux maxima can be obtained by assuming that particle fluxes are determined by a balance between radial diffusion and supply by the CRAND process. The Van Allen study was directed toward an investigation of the G Ring including limits on particulate sizes as well as on column mass density. His quantitative analysis did not utilize the phase space density data of Figure 1 but consisted of a direct analysis of

observed counting rates because of their improved spatial resolution. Model calculations were performed using a relatively simple one-dimensional diffusion equation for the number density $N$ in a time-stationary situation,

$$D\frac{d^2N}{dr^2} = -S \tag{1}$$

where $D$ is the diffusion rate and S is the source rate (both assumed constant). In order for (1) to be a valid description, it is necessary that particle losses be negligible and that the particle energy remain constant during inward or outward diffusion. The latter condition can be true only to a first approximation within a limited radial range since conservation of the first adiabatic invariant requires that the particle energy change with radial distance in the planetary magnetic field. Nevertheless, since the observed counting rates were obtained by integral detectors (e.g. energies > 80 MeV in the case of the profile of Figure 2) and the radial range of application is small (several tenths of an $R_S$), equation (1) provides a reasonable description for this application. The parabolic fit to the largest peak in Figure 2 was obtained by Van Allen using solutions of (1) for a ratio of source strength to diffusion rate of $S/D = 6.9 \times 10^{-24}$ cm$^{-5}$. Using theoretical estimates for the source strength at $r = 2.67$ $R_S$, a diffusion rate of $D \sim 1.3 - 2.8 \times 10^{-11}$ $R_S{}^2$ s$^{-1}$ was inferred for these particles at this radial distance. From the observed changes in slope of the counting rate profile in the vicinity of Ring G and from the inferred ratio of $S/D$, a maximum lifetime of 1.6-3.5 years for > 80 MeV protons against absorption by the G ring was calculated. According to the model of Thomsen and Van Allen [1979; see section 3], the particle lifetime $\tau$ against absorption by a particulate ring is related to the column mass density of the ring, $\sigma$, by

$$\sigma = \rho R\left(\frac{T_B}{2\tau}\right)(\cos\alpha_e)\left(\frac{2r_g}{\Delta r}\right)$$

where $\rho$ is the particulate mass density ($\sim$ 1 gm/cm$^3$), $T_B$ is the energetic particle latitudinal bounce period, $\alpha_e$ is the equatorial pitch angle, $R$ is the stopping distance or range (in cm) of the energetic particle in ring material, $r_g$ is the particle gyroradius, and $\Delta r$ is the radial width of the ring. Choosing typical values of $T_B \sim 3$ sec, $\cos\alpha_e = 0.4$, $R \sim 25$ cm, $r_g \sim 5000$ km, and $\Delta r \sim 1000$ km, Van Allen estimated a lower limit on the column mass density of $\sigma \simeq 1.4 \times 10^{-6}$ gm/cm$^2$ for Ring G. The column mass density can in turn be used to estimate the mean ring particle thickness $\bar{t}$ provided that the normal opacity $\eta$ of the ring is known:

$$\bar{t} = \sigma/(\rho\eta)$$

Taking a typical estimate for $\eta$ of $3 \times 10^{-5}$, Van Allen obtained a lower limit on the mean thickness of Ring G particulates of $\bar{t} > 450$ $\mu$m. For spherical particles, the corresponding limit on the mean particulate radius is > 350 $\mu$m. If uncertainties in ring radial width

and normal opacity are excluded for the moment (see below), remaining uncertainties in CRAND proton source rate, energy spectrum, effective gyroradius, and inferred radial diffusion rate imply that these calculated lower bounds should be considered as valid to the order of magnitude only, i.e. hundreds of $\mu$m for the particulate size.

The derived bound on the mean particulate thickness implies a corresponding bound on the size distribution of particulates in the ring given by

$$\bar{t} = (4/3)\langle r^3 \rangle / \langle r^2 \rangle$$

where $r$ is the radius of a single particulate (assumed spherical) and the angle brackets denote the mean over the distribution.

Recent work using optical data sets by M. Showalter presented at the last Cassini dust environment workshop indicated significant revisions in the preferred values of both the radial width $\Delta r$ and the normal opacity $\eta$ for Ring G. Specifically, $\eta$ is revised downward to $\sim 10^{-6}$ while $\Delta r$ is revised upward to 7000-8000 km. The upward revision of $\Delta r$ has the effect of lowering the column density estimated by Van Allen [1983] by a factor of 7-8 to $\sim 2 \times 10^{-7}$ gm/cm$^2$. The combination of a downward revision of $\eta$ by a factor of $\sim 30$ and an upward revision of $\Delta r$ by a factor of 7-8 increases the mean particulate size estimate by a factor of $\sim 4$. Therefore, Van Allen's [1983] particulate size estimate of several hundred $\mu$m could be revised upward to a value of the order of $10^3$ $\mu$m. In summary, the best available estimate for the column mass density of Ring G is $\sim 2 \times 10^{-7}$ gm/cm$^2$ and the best estimate for the mean particulate thickness is $\sim 10^3$ $\mu$m.

Column Mass Density Limits at 2.43 and 2.67 $R_S$

As noted above, CRAND proton fluxes maximize at several radial locations in the inner zone including at $\sim 2.43$ $R_S$ and $\sim 2.67$ $R_S$. For the purpose of providing constraints on Cassini mission planning, we seek to determine limits on the column mass density of solid material within radial ranges centered on these maxima. The analysis proceeds along the lines of Van Allen's [1983] study but allows for the possibility of particle losses as well as sources near flux maxima.

A simple upper bound on the mean column mass density of material near the two inner zone peaks of Figure 2 may be obtained from the condition that the source strength (production rate) of CRAND protons must exceed the loss rate due to absorption by solid material near a flux maximum. This condition follows from the one-dimensional stationary diffusion equation with a non-zero loss rate $\mathcal{L}$,

$$D\frac{d^2N}{dr^2} + \mathcal{S} - \mathcal{L} = 0$$

Within the small radial ranges considered, $D$, $\mathcal{S}$, and $\mathcal{L}$ are assumed to be constant. Since the number density $N$ is proportional to the particle omnidirectional flux $J$ (and therefore the counting rate for the data of Figure 2), the 1-D diffusion equation reduces to

$$\frac{d^2 J}{dr^2} = -(S - \mathcal{L})/D$$

From this form, any radial zone in which the flux profile has negative curvature will contain more sources than sinks of particles, irrespective of the value of the diffusion coefficient $D$. The maxima centered on 2.43 and 2.67 $R_S$ clearly have negative curvature. Therefore, we have

$$\mathcal{L} < S$$

at both of these maxima. The source strength $S$ of CRAND protons with energy > 80 MeV can be estimated theoretically from the production rate model calculations of Cooper [1983] and Blake et al. [1983], which are in substantial agreement with one another. Flux injection rates calculated by Cooper [1983] are shown in Figure 3. By interpolation, we find

$$S(2.43) \simeq 9 \times 10^{-5} \ (\mathrm{cm}^{-2}\mathrm{s}^{-1})\mathrm{s}^{-1}$$

$$S(2.67) \simeq 6 \times 10^{-5} \ (\mathrm{cm}^{-2}\mathrm{s}^{-1})\mathrm{s}^{-1}$$

Thus the loss rates at 2.43 and 2.67 $R_S$ must be less than these source rates.

In order to determine corresponding upper limits on column mass density, it is necessary to convert the above loss rate limits to limits on the particle lifetime against absorption. To do this, we first translate the counting rates for > 80 MeV protons into approximate omnidirectional fluxes using instrument geometric factors given by Van Allen et al. [1980]. The result is shown in Figure 4 for the counting rates of Figure 2. Also plotted for comparison are omnidirectional fluxes estimated for > 80 MeV protons from measurements by the UCSD detector on Pioneer 11 [Fillius et al., 1980]. The estimated peak fluxes are in approximate agreement indicating that the absolute magnitudes of the peak fluxes are not a major source of error in the analysis. The Iowa data will be used for quantitative modeling studies below because of its greater spatial resolution. The peak fluxes estimated from the Iowa measurements are $J(2.43) \sim 8000 \ \mathrm{cm}^{-2}\mathrm{s}^{-1}$ and $J(2.67) \sim 27000 \ \mathrm{cm}^{-2} \ \mathrm{s}^{-1}$. The loss rate near the peaks may be approximated as

$$\mathcal{L} \sim J(\mathrm{peak})/\tau$$

where $\tau$ is the particle lifetime against absorption by solid matter. Then the corresponding lower limits on the particle lifetime are

$$\tau(2.43) > 8.9 \times 10^7 \ \mathrm{sec}$$

$$\tau(2.67) > 4.5 \times 10^8 \text{ sec}$$

It should be noted that the limit on $\tau$ at 2.67 $R_S$ is substantially larger than that at 2.43 $R_S$ because of the difference in peak fluxes even though the limits on $\mathcal{L}$ at these two locations were nearly the same.

The charged particle lifetime against absorption by a ring of material with radial width $\Delta r$ may be written as [Van Allen, 1983],

$$\tau = \frac{\rho R}{\sigma}\left(\frac{T_B}{2}\right)\left(\frac{2r_g}{\Delta r}\right)\cos(\alpha_e$$

where $\sigma$ is again the column mass density. For > 80 MeV protons (mean energy $\sim$ 200 MeV), we have $R \sim 26$ cm, $2r_g \sim 3000 - 4000$ km, $\cos\alpha_e \sim 0.2$, and $T_B \sim 3$ seconds. If we assume that $\Delta r \geq 2r_g$, then the corresponding upper limits on areal mass density are:

$$\sigma(2.43) < 9 \times 10^{-8} \text{ g cm}^{-2}$$

and

$$\sigma(2.67) < 2 \times 10^{-8} \text{ g cm}^{-2}$$

These upper limits are both less than the lower limit on column mass density for the G Ring derived above ($\sigma$(G Ring) > $2 \times 10^{-7}$ gm/cm$^2$) using the revised radial width estimated from optical measurements by Showalter.

In order to determine more restrictive upper limits on the column mass densities at 2.43 and 2.67 $R_S$, it is necessary to consider solutions of the full 1-D diffusion equation. Replacing the loss rate $\mathcal{L}$ with $J/\tau$,

$$D\frac{d^2J}{dr^2} + S - J/\tau = 0.$$

Within a small radial range for which $D$, $S$, and $\tau$ are approximately constant, the general solution is

$$J(r) = A\exp[r/(D\tau)^{\frac{1}{2}}] + B\exp[-r/(D\tau)^{\frac{1}{2}}] + S\tau$$

At this point, several approaches may be taken in order to construct model profiles for comparison with the data of Figure 4. The most general approach would involve dividing the entire radial range between 2.4 and 3.1 $R_S$ into a series of layers with specific undetermined values of $D$ and $\tau$ for each layer. Application of appropriate boundary conditions between layers (continuity of $J$ and $\partial J/\partial r$) would then allow construction of a composite solution valid over the entire radial range. However, the number of undetermined parameters would be large so it is questionable whether this procedure would be successful in

allowing more restrictive constraints on the column mass density near the two inner peaks. This is especially true in view of the fact that there are few if any independent constraints on the amplitude and r-dependence of $D$ for CRAND protons in the inner zone.

An alternate approach that we take here is to consider only the specific regions of interest centered on 2.43 and 2.67 $R_S$. Within these zones, the maximum particle flux and the radial location of the peak flux are known. Denoting the radial location of the peak flux as $a$, two observational constraints on the flux profile within these regions are:

$$J = J(a) \text{ and } \frac{dJ}{dr} = 0 \text{ at } r = a$$

Subject to these constraints, the solution becomes

$$J(r) = [J(a) - S\tau]\cosh\left(\frac{r-a}{(D\tau)^{\frac{1}{2}}}\right) + S\tau$$

Note that for the special case $J(a) = S\tau$ (equivalent to the upper bound on the loss rate discussed above), $J(r)$ is a constant equal to the peak flux. The value of $\tau$ for which this is the case is denoted $\tau_{crit}$. As stated earlier, $\tau_{crit}(2.43) \simeq 8.9 \times 10^7$ seconds and $\tau_{crit}(2.67) \simeq 4.5 \times 10^8$ seconds. However, for larger $\tau$ values such that $J(a) - S\tau$ is negative, $J(r)$ decreases with radial distance away from $r = a$. The extent of the negative curvature depends on the combined values of $\tau$ and $D$ (assuming that $S$ is known).

Since the value of $D$ is unconstrained, the only method of analysis is to assume values of $\tau$ and determine the value of $D$ that produces an optimal fit to the flux profile. Values of $\tau \leq \tau_{crit}$ result in very poor fits to the data for any assumed value for $D$. However, as $\tau$ is increased to successively larger values, values for $D$ are found that produce better and better fits to the observed flux profile. When the model profile agrees with the observed profile to within data uncertainties, then the desired improved lower limit on $\tau$ (and hence an improved upper limit on the column mass density) is obtained. Figure 5 shows graphically the result of applying this procedure to the Pioneer 11 Iowa data of Figure 4. Figure 5a shows the model profile for the special case of $\tau = \tau_{crit}$ while Figure 5b is for $\tau$-values slightly larger than $\tau_{crit}$. Similarly, Figures 5c-5d show optimal fits to the flux profile for successively larger $\tau$ values. The optimal value of $D$ in each case is determined by varying $D$ until a minimum in the rms deviation between the model profile and the data profile is reached. In the case of the maximum at 2.67 $R_S$, the fit is limited to radial distances less than 2.75 $R_S$ to avoid slope changes that may be associated with Ring G absorption. Figure 6 plots the rms deviation corresponding to the optimal $D$ value for $\tau$-values increasing from $\tau_{crit}$.

It is evident from either Figure 5 or Figure 6 that the model fits become imperceptibly different from the data profiles for $\tau(2.43)$ greater than about $2 - 3 \times 10^8$ seconds and for $\tau(2.67)$ greater than about $1 \times 10^9$ seconds. Both profile maxima are *consistent* with no absorption losses. That is, as $\tau$ is increased to infinity, the rms deviation asymptotically approaches a minimum. However, given the uncertainties in the data profile alone, lifetimes significantly larger than the above values can not be excluded. These preferred maximum

lifetimes are only a factor of 2-3 larger than the lower bound derived from the condition that $\mathcal{L} < \mathcal{S}$. They result in corresponding increases of the derived upper bounds on column mass densities to:

$$\sigma(2.43) < 4 \times 10^{-8} \text{ gm cm}^{-2}$$

and

$$\sigma(2.67) < 1 \times 10^{-8} \text{ gm cm}^{-2}$$

Both of these upper limits are significantly less than the lower limit on the column mass density of the G Ring given above ($\sim 2 \times 10^{-7}$ gm/cm$^2$). It is doubtful that these limits can be lowered significantly with further modeling of the Iowa data of Figure 4 due to the fact that the diffusion rate is not independently constrained. It is clear that the G Ring produces only a relatively gentle reduction in the particle flux. It is therefore not surprising that these CRAND proton fluxes can not usefully distinguish column densities much lower than an order of magnitude less than that of the G Ring.

Although the upper limit on the loss rate of CRAND protons is not greatly different between the 2.43 and 2.67 $R_S$ flux peaks, the inferred column mass density upper limits do differ significantly (by a factor of about 4) due primarily to the larger flux maximum at the 2.67 $R_S$ location. Thus the 2.67 $R_S$ location is preferable from the standpoint of minimum risk as expected qualitatively from the discussion relating to Figure 1. The extent to which either the 2.43 $R_S$ location or the 2.67 $R_S$ location may be acceptable for the Cassini SOI is a matter for the project to decide based on the column mass density upper limits derived above.

## 2. Brief Review of Relevant Satellite Absorption Microsignatures

Carbary et al. [1983] discussed and analyzed a series of apparent absorption microsignatures in measurements by the low energy charged particle (LECP) instruments on Voyagers 1 and 2 during the respective Saturn flybys. Most of the observed microsignatures were directly attributable to absorption by the known satellites. However, at the orbital distances of Mimas and Enceladus, microsignatures were observed that were not easily attributed to satellite absorption. In this section, we briefly review the evidence for microsignatures that may suggest the existence of low-optical-depth debris clouds co-orbiting with these satellites. This issue is of interest in evaluating the hazard of repeated crossings of inner satellite orbits by the Cassini orbiter.

The Voyager 2 "Enceladus" microsignature occurred when the spacecraft was about 20° behind the satellite in azimuth and was present in all electron and ion channels (Figure 7). This location is on the wrong side of Enceladus to be due to absorption of ions or corotation dominated electrons (energies < 1 MeV) unless a very long lifetime against both radial diffusion and dispersion effects is assumed. In addition, the temporal width of 150 s observed in all channels corresponds to a distance in the equatorial plane of 2640 km. This distance is much greater than the expected value of the satellite diameter (500 km) plus twice the particle gyroradius (< 50 km), again suggesting that Enceladus is not

the source of the microsignature. A possible explanation for the microsignature that does not require additional material in orbit with Enceladus is that the LECP detectors were actually observing a decrease in very energetic electrons that would drift retrograde relative to the satellite orbit motion. However, Carbary et al. presented evidence to the contrary and concluded that energetic electron contamination could account for a maximum of 3% of the observed $\sim$ 28% ion counting rate decrease. Since Enceladus' orbit occurs near the maximum optical thickness of the E ring and may represent the source of Ring E particulates [e.g. Cuzzi et al., 1984], it was suggested by Carbary et al. that low optical depth clumping of Ring E material may represent the most plausible explanation of the microsignature.

The Voyager 2 "Mimas" microsignature was detected by both the LECP and CRS instruments [Carbary et al., 1983; Vogt et al., 1982] on the outbound pass when the spacecraft was approximately 147° ahead of Mimas in its orbit (Figure 8). The lack of a similar microsignature on the inbound pass when the spacecraft was $\sim$ 127° ahead of the satellite combined with the detailed characteristics of the microsignature led both Carbary et al. and Vogt et al. to suggest that the microsignature was produced by an unknown absorbing satellite or clump of material.

In this context, it should be mentioned that a recent study of Pioneer 11 electron flux microsignatures near the F ring has obtained evidence for a series of low optical depth clumps of material in orbit between the shepherding satellites Pandora and Prometheus [Cuzzi and Burns, 1988]. These clumps of material are hypothesized to be produced transiently by accumulation of debris from collisions of unseen (0.1–10 km radius) parent objects. If so, then the Mimas and Enceladus microsignatures could imply the existence of similar unseen moonlets and/or debris clouds in orbit with these inner satellites. Because the longitudinal extent and optical depth of these suspected clouds of particulates is unknown, a detailed modeling analysis to infer probable sizes of particulates and column densities may not be justified at this stage. However, at a minimum, these observations indicate the need to monitor energetic particle fluxes and angular distributions during the Cassini orbiter mission phase in order to continuously evaluate the hazard to the spacecraft during near-satellite passes.

## 3. E Ring Absorption of Low Energy Electrons

### Ring Absorption Models

Prior to the Pioneer 11 Saturn encounter, Thomsen and Van Allen [1979] described various methods by which measurements of trapped energetic particles could be applied to infer properties of Ring E, including mean particle size. Although the details of their calculations are not specifically relevant here, their general approach is still applicable and has already been applied, in part, by Van Allen [1983] in his study of absorption of CRAND protons by the G ring.

For particles whose latitudinal bounce period and equatorial pitch angle are known, the particle lifetime against Ring E absorption can be estimated as follows. First, the *mean encounter time* for a single ion or electron with a single ring particle is

$$t_{me} = \left(\frac{T_B}{2}\right)(\cos \alpha_e)\left(\frac{1}{\eta}\right)$$

where $T_B$ is the latitudinal bounce period of the charged particle; $\alpha_e$ is the equatorial pitch angle; and $\eta$ is the ring optical depth, assumed to be much less than unity. For this relation to be valid, it is necessary that the charged particle mirror latitude be greater than the latitudinal extent of the ring, a good approximation even for the latitudinally thick E ring except for particles with $\alpha_e$ of nearly 90°.

If the range $R$ of an energetic ion or electron in ring material (Figure 9) is less than the mean ring particle thickness $\bar{t}$, then the mean encounter time is the same as the mean charged particle lifetime $\tau$ against ring absorption:

$$\tau = t_{me} \qquad (R \leq \bar{t}) \tag{5}$$

If not, then the lifetime is increased by an amount that can be estimated roughly by the ratio of the range to the mean particle thickness:

$$\tau = t_{me}\left(\frac{R}{\bar{t}}\right) \qquad (R > \bar{t}) \tag{6}$$

In practice, there is also a gradual energy loss for charged particles with ranges much greater than ring particle thicknesses as they repeatedly encounter ring particles. The probability of an actual absorption of a radially diffusing charged particle depends on the ratio of the absorption lifetime to the diffusion time $t_D$ required for the particle to diffuse radially across the L-range occupied by the ring. The probability approaches unity when $\tau \leq t_D$.

Observational Evidence for Ring E Absorption

Sittler et al. [1981] reported a general extinction of suprathermal electrons with energies < 6 keV measured with the Voyager 1 plasma science instrument inside 7-8 $R_S$ that was interpreted as due to E Ring absorption. Within this general extinction signature, a stronger reduction in suprathermal electron flux was observed inside L-values of about 5 with maximum depletion near the minimum L-value of 4.35. The latter depletion was interpreted to be a result of an enhancement of particulates near Enceladus. It was noted that these extinctions of suprathermal electrons could in principle also be explained by interactions with neutral gas having column densities as large as $10^12$ cm$-2$; however, the lack of evidence for such large column densities from the Voyager UV measurements was used to discount this option. Another alternate model for depletion of these electrons that is more difficult to eliminate involves interactions with possible whistler-mode waves in the Tethys-Dione-Rhea ion torus [E. Sittler, private communication].

Direct evidence for Ring E absorption of more energetic trapped particles in the inner Saturnian magnetosphere based on Pioneer 11 and Voyager energetic particle detector measurements has been somewhat ambiguous, especially for ions. For example, Hood

[1985; 1989] showed that the decline of energetic proton phase space densities inward of $L$ = 10 may be explained by pitch angle scattering losses as well as by satellite and Ring E absorption. Similarly, $\sim$ 1 MeV proton flux measurements show a general decline inward of $L = 7$, reaching an apparent minimum at $L \simeq 4$. However, it is not possible to clearly associate this minimum with the location of the E ring optical depth maximum because of contamination by higher-energy (CRAND) protons inward of $L = 4$.

The situation with respect to energetic electron measurements is more encouraging. Shown in Figure 10 are integral energetic electron fluxes measured with the University of Iowa instrument on Pioneer 11 [Van Allen, 1984]. A substantial dip occurs in the $>$ 0.04 MeV flux centered on a distance of about 5 $R_S$ while the $>$ 0.56 MeV flux shows no substantial decrease. Comparing the flux profiles for $E >$ 0.04 MeV and $E >$ 0.56 MeV (note that the scales differ by one order of magnitude), it is evident that there are no electrons (within instrumental uncertainties) with $0.04 < E < 0.56$ MeV inside of $L \simeq 5$. These electrons are lost primarily inside of $L \sim 7$. Figure 11 compares the inbound and outbound profiles for $E >$ 0.04 MeV; the similarity of the integral flux minima indicates that they are a time-independent property of low-energy electrons in this zone. Energetic electron omnidirectional counting rates observed during the outbound trajectory of Voyager 2 by the Low Energy Charged Particle (LECP) instrument are reproduced in Figure 12. Flux reductions inside L = 7-8 in the intensities of electrons with energies less than about 800 keV are again evident. However, the increased energy resolution of the Voyager measurements appears to reveal also a slight increase of low-energy electron fluxes inside L = 4-5 (see the discussion by Van Allen, 1984). The latter increase could be attributed in part to a local internal source of such electrons but low-resolution phase space density profiles for LECP electrons calculated by Armstrong et al. [1983] provide evidence for electron sources only at higher energies.

The energy dependence of the observed LECP counting rate minima (stronger minima with decreasing energy) could be consistent with losses due to absorption by the E Ring because the range $R$ of these electrons increases with increasing electron energy (Figure 9). Thus it is possible that the lower-energy electrons are experiencing stronger E ring absorption losses than are those at higher energies. If so, then the observed flux declines between $\sim$ 7 $R_S$ and $\sim$ 4 $R_S$ could be attributed largely to Ring E absorption. In support of this suggestion, Grosskreutz [1982] reported analyses of Pioneer 11 Iowa detector A electron pitch angle distributions indicating preferential losses of nearly equatorially mirroring electrons inside $L = 7$. Figure 13 is a plot of the ratio of the maximum counting rate observed at any pitch angle to that observed at $\alpha_e = 89°$. Inside $L \sim 7$, the flux of particles with $\alpha_e$ near 90° appear to be progressively reduced. The maximum depletion occurs between 3 and 5 $R_S$ where the optical depth of the E ring is a maximum. She therefore concluded that "this similarity is suggestive of the role of the E Ring in affecting the angular distributions".

It should be noted that there is a question of whether the counting rate data of Figure 12 could be partially contaminated by penetrating, higher-energy particles inward of 4 $R_S$ (J. F. Cooper, private communication). If so, then the flux increases occurring inward of 4 $R_S$ could be partly or entirely artificial (although LECP investigators have argued that contamination is unlikely). In any case, the flux *decreases* occurring with decreasing radial

distance outside 4 $R_S$ imply losses that still must be explained. In the next paragraph, we estimate the implied loss rate and calculate corresponding energetic particle lifetimes assuming that all of the losses occurring between 5 and 4 $R_S$ are due to Ring E absorption. If other magnetospheric loss processes (e.g. charge exchange, wave-particle interactions) are operative in this region, these inferred loss rates will represent an upper limit on the rate of E Ring absorption.

E Ring Parameter Estimates

In the following, it is assumed that the observed lower-energy electron flux reductions inside L = 6-7 are a consequence of direct absorption by Ring E particulates. Under this assumption, several approaches may be taken to estimate gross properties of the ring using the model of Thomsen and Van Allen [1979]. Barring measurement errors or strong physical electron sources that would conceal absorption signatures in higher-energy electrons, such an analysis should at least yield an upper limit on the column mass density and mean size of particulates within the E Ring.

The simplest, and least model dependent, approach follows from the condition stated earlier that an absorption macrosignature in particle flux measurements can occur only if the lifetime $\tau$ of the particles against absorption is comparable to or less than the time $\tau_D$ required for particles to diffuse radially across the absorbing region. If $\Delta L$ is the radial width of the absorbing region, then this condition can be expressed as

$$\frac{\tau}{\tau_D} < 1 \quad \text{or} \quad \frac{\tau D}{\Delta L^2} < 1$$

where $D$ is again the radial diffusion coefficient for the particles in question. According to the Voyager 2 counting rate data of Figure 12, $\Delta L$ is of order unity and significant flux minima begin to occur at a particle energy of about 500 keV. Consequently, we expect that $\tau D$ becomes of the order of or less than unity for electrons of this energy at L = 4-5 $R_S$.

A slightly more quantitative, but more model-dependent, approach utilizes solutions of the time-stationary 1-D radial diffusion equation in order to simulate the flux dips in the data of Figure 12. We emphasize at the outset that this equation is valid only over limited radial ranges for which the change in the magnetic field $B$, and hence the particle energy (by conservation of the first invariant), can be neglected. The validity of this approximation is improved somewhat when analyzing data from integral particle detectors that measure the flux of particles over a finite range of energies. Specifically, the Voyager LECP electron energy ranges are typically a factor of 2 or more from minimum to maximum (Figure 12). For particles conserving the first invariant $\mu$, the particle energy is changed by a factor of 2 during radial transport across about 1 $R_S$ at a distance of 4 $R_S$. Thus, the particle energy is changed beyond the bandpass of the detector energy channel only during inward or outward diffusion through a radial distance of $> 1$ $R_S$. A 1-D diffusion formulation is therefore expected to be valid to first order over a radial distance of $\leq 1$ $R_S$. The appropriate diffusion equation is

$$D\frac{d^2J}{dr^2} - J/\tau = 0.$$

where J is the measured omnidirectional flux or counting rate. For the case in which $D$ and $\tau$ are constant, the solution can be written in the form

$$J(r) = J(a)\cosh\left(\frac{r-a}{(D\tau)^{\frac{1}{2}}}\right)$$

where $a$ is the radial distance where the flux reaches a minimum ($dJ/dr = 0$). Figure 14 shows best-fitting profiles and corresponding values of $\tau D$ for the four top profiles with distinct flux minima. The rms fit was limited to the portion of the profile between the flux minimum and a distance of 1 $R_S$ outside the minimum. This was done to avoid the region inward of 4 $R_S$ where contamination of the counting rates by higher-energy CRAND protons could have occurred. It is seen that the inferred values for $\tau D$ decrease with decreasing particle energy and are less than unity where macrosignatures are present, as expected from the qualitative treatment above. It is therefore concluded that the product $\tau D$ must decrease below unity for electrons with energies below approximately 500 keV. Due to uncertainties in $D$ and its dependence on electron energy (see below), no more detailed analysis to more precisely constrain the product $\tau D$ has been attempted.

In order to estimate the lifetime $\tau$, it is necessary to have independent constraints on the diffusion coefficient $D$. Figure 15 summarizes a series of data-derived estimates for the amplitude and L-dependence of $D$ for low-energy (co-rotation dominated) ions and electrons. The individual squares and circles are derived from analyses of observed satellite microsignatures in particle flux measurements using a one-dimensional time-dependent diffusion equation [Hood, 1985; Carbary et al., 1983]. In reality, some 'smear' due to energy and pitch angle dispersion contributes to the evolution of satellite microsignatures. Consequently, at least some of these microsignature-derived estimates for $D$ may actually represent upper limits. The solid lines represent model fits to phase space density profiles for low-energy ions derived from Voyager LECP data for a series of possible loss models ranging from satellite absorption only (curve a) to solid body absorption plus strong pitch angle diffusion losses (curve d) [Hood, 1985]. When both the microsignature-derived $D$ values and the model $D$ profiles are considered, the most probable range for $D$ near L = 4-5 is $10^{-9}$ to $10^{-8}$ $R_S{}^2$ $s^{-1}$.

Using the estimated range for $D$, the lifetime against Ring E absorption for electrons with energy $\sim$ 500 keV at 4-5 $R_S$ is estimated as

$$\tau \sim 10^8 \text{ to } 10^9 \text{ sec}$$

From the Ring E loss model of Thomsen and Van Allen [1979], the column mass density $\sigma$ is given by

$$\sigma = \rho\bar{t}\eta = \frac{\rho R}{\tau}\frac{T_B}{2}\cos\alpha_e$$

Taking values of $R \simeq 0.1$ cm (Figure 9), $T_B \simeq 5$ seconds, $\cos \alpha_e \simeq 0.2$, then

$$\sigma \sim 5 \times 10^{-10} \text{ to } 5 \times 10^{-11} \text{ gm/cm}^2$$

Since the normal opacity of the E Ring can be independently constrained from ground-based and Voyager imaging, it is also possible to estimate corresponding limits on the mean ring particle thickness. Although the maximum optical thickness has been estimated as greater than $10^{-6}$ near the orbit of Enceladus, a more appropriate mean value for the 4-5 $R_S$ region is $\sim 5 \times 10^{-7}$ [S. Larson and M. Showalter, private communications]. Thus,

$$\bar{t} = \sigma/(\rho\eta) \sim 1 \text{ to } 10 \ \mu\text{m}$$

The corresponding constraint on the size distribution of Ring E particulates is given by the relation [e.g. Van Allen, 1983],

$$\bar{t} = (4/3)\langle r^3 \rangle / \langle r^2 \rangle$$

where $r$ is the radius of a single particulate (assumed spherical) and the angle brackets denote the mean over the distribution.

Phase Space Density Models

In principle, radial phase space density profiles of low-energy electrons in the inner Saturnian magnetosphere would allow rigorous modeling to infer absorption lifetimes within a lossy region for a given form of the diffusion coefficient $D$. Unfortunately, profiles at sufficiently low energies with adequate resolution to show a reduction in accord with the flux minima evident in Figure 12 do not appear to be available.

Phase space density profiles for energetic electrons in Saturn's inner magnetosphere have been published by Van Allen et al. [1980] and Armstrong et al. [1983]. The Van Allen et al. profile (Figure 16) is for equatorially mirroring, energetic (525 MeV/G) electrons with integral invariant $K \sim 0$. At $L \sim 4$, these electrons have energies of nearly 1 MeV and are therefore not subject to strong E Ring absorption losses according to Figures 11 and 12. The Armstrong et al. profiles for $\mu < 80$ MeV/G and $K = 0.28$ G$^{\frac{1}{2}}$R$_s$ decline rapidly inside $L = 6$-7, consistent with possible Ring E and satellite absorption losses. At higher energies, some evidence for a finite electron source inside $L = 4.5$ was obtained in the form of an inward increase of the calculated phase space densities. In general, the Armstrong et al. Voyager 2 phase space density profiles are relatively low in spatial resolution. No change in slope is discernible on these profiles that could be attributed to a Ring E absorption macrosignature despite the pronounced minima evident at lower energies in Figure 12. Consequently, it is not possible to apply them to estimate the Ring E loss rate for given assumptions about the radial diffusion rate of these electrons. Further, more refined calculations of Saturn electron phase space densities based on Voyager measurements are planned but will not be completed in the near future [A.F. Cheng, private communication].

In the interim, we present here an analysis of the Van Allen et al. [1980] 525 MeV/G equatorially mirroring electron profile using macroscopic diffusion and loss models similar to those employed by Hood [1985; 1989]. Before doing so, it should be emphasized that some uncertainty in this profile exists due to the particular energy spectrum that was adopted by Van Allen et al. (illustrated in Figure 16). This energy spectrum is characterized by a low energy cut-off that was motivated in part by the apparent absence of electrons with energies less than 0.04 MeV inside L = 5 (Figure 10). However, as discussed earlier, the Voyager LECP instruments have measured finite fluxes of low-energy electrons that appear to contradict the Pioneer 11 measurements. In addition to these uncertainties, it is questionable whether electrons of these higher energies are experiencing substantial Ring E losses, as noted above. Nevertheless, since this is the only published Pioneer 11 electron phase space density profile relevant for the investigation of E Ring losses, we have carried out the appropriate model calculations.

Shown in Figure 17 is the result of this exercise. In each case, a particular loss model was assumed and the corresponding form of the radial diffusion coefficient $D(L)$ (assumed to obey a power law in $L$) was determined by a minimum variance fit to the observed phase space densities. In the top panel, a loss model consisting of satellite absorption only was employed. Large satellite absorption macrosignatures are present in the model phase space densities that are not present in the data profiles. This indicates a need for additional losses distributed among the satellites. These losses could in principle consist of Ring E absorption or of magnetospheric losses resulting from wave-particle interactions. From the pitch angle distributions analyzed by Grosskreutz [1982; see above], it was inferred that Ring E absorption is the most probable dominant loss process. Thus the models in the middle and lower panels of Figure 17 include Ring E absorption losses for particular mean ring particle radii of 10 and 100 $\mu$m, respectively. As expected, the additional distributed losses do reduce the amplitude of the satellite macrosignatures and yield improved fits to the phase space densities as measured by the RMS parameter. Taken at face value, this result would indicate mean Ring E particulate sizes in excess of 100 $\mu$m. For nominal optical thicknesses of $5 \times 10^{-7}$, column mass densities in excess of $5 \times 10^{-9}$ gm/cm$^2$ would be implied. However, such an inference depends primarily on the absence of satellite absorption macrosignatures in the data profiles. Because the actual form of the phase space density profile is uncertain (due to the assumed energy spectrum), as is its actual spatial resolution, this result is not regarded as a strong constraint.

## 4. References


Armstrong, T.P., M.T. Paonessa, E.V. Bell II, and S.M. Krimigis, Voyager observations of Saturnian ion and electron phase space densities, *J. Geophys. Res., 88*, 8893-8904, 1983.

Blake, J.B., H. Hilton, and S.H. Margolis, On the injection of cosmic ray secondaries into the inner Saturnian magnetosphere, 1. Protons from the CRAND process, *J. Geophys. Res., 88*, 803-807, 1983.

Carbary, J. F., S.M. Krimigis, and W.H. Ip, Energetic particle microsignatures of Saturn's satellites, *J. Geophys. Res., 88*, 8947-8958, 1983.

Cooper, J.F., Nuclear cascades in Saturn's rings: Cosmic ray albedo neutron decay and origins of trapped protons in the inner magnetosphere, *J. Geophys. Res., 88*, 3945-3954, 1983.

Cuzzi, J.N. and J.A. Burns (1988) Charged particle depletion surrounding Saturn's F ring: Evidence for a moonlet belt, *Icarus, 74*, 284-324, 1988.

Cuzzi, J.N., J.J. Lissauer, L.W. Esposito, J.B. Holberg, E.A. Marouf, G.L. Tyler, and A. Boischot, Saturn's rings: Properties and processes, in *Planetary Rings*, edited by R. Greenberg and A. Brahic, University of Arizona Press, Tucson, p. 73-199, 1984.

Fillius, W., W.-H. Ip, and C.E. McIlwain, Trapped radiation belts at Saturn: First look, *Science, 207*, 425-430, 1980.

Grosskreutz, C.L., Distribution of energetic electrons ($0.040 < E_e < 21$ MeV) in Saturn's inner magnetosphere, M.S. Thesis, 48 pp., Department of Physics, University of Iowa, 1982.

Hood, L. L., Radial diffusion of low-energy ions in Saturn's radiation belts: A combined analysis of phase space density and satellite microsignature data, *J. Geophys. Res., 90*, 6295-6303, 1985.

Hood, L. L., Radial diffusion and losses of energetic protons in the 5 to 12 $R_S$ region of Saturn's magnetosphere, *J. Geophys. Res.*, in press, 1989.

Krimigis, S.M., T.P. Armstrong, W.I. Axford, C.O. Bostrom, G. Gloeckler, E. P. Keath, L.J. Lanzerotti, J.F. Carbary, D.C. Hamilton, and E.C. Roelof, Low-energy charged particles in Saturn's magnetosphere: Results from Voyager 1, *Science, 212*,225-230, 1981.

Roederer, J.G., *Dynamics of Geomagnetically Trapped Radiation*, 166 pp, Springer-Verlag, New York, 1970.

Schulz, M. and L.J. Lanzerotti, *Particle Diffusion in the Radiation Belts*, 215 pp, Springer-Verlag, New York, 1974.

Sittler, E.C., Jr., J.D. Scudder, and H.S. Bridge, Distribution of neutral gas and dust near Saturn, *Nature, 292*, 711-714, 1981.

Thomsen, M.F. and Van Allen, J.A., On the inference of properties of Saturn's Ring E from energetic charged particle observations, *Geophys. Res. Lett., 6*, 893-896, 1979.

Van Allen, J. A., Absorption of energetic protons by Saturn's Ring G, *J. Geophys. Res., 88*, 6911-6918, 1983.

Van Allen, J. A., Energetic particles in the inner magnetosphere of Saturn, in *Saturn*, edited by T. Gehrels and M. Matthews, pp. 281-317, University of Arizona Press, Tucson, 1984.

Van Allen, J.A., Randall, B.A., Thomsen, M.F., Sources and sinks of energetic electrons and protons in Saturn's magnetosphere, *J. Geophys. Res., 85*, 5679-5694, 1980.

Vogt, R. E., D. L. Chenette, A. C. Cummings, T. L. Garrard, E. C. Stone, A. W. Schardt, J. H. Trainor, N. Lal, and F. B. McDonald, Energetic charged particles in Saturn's magnetosphere: Voyager 2 results, *Science, 215*, 577-580, 1982.

## Figure Captions

Figure 1. Radial dependence of phase space density (in arbitrary units) of equatorially mirroring CRAND protons derived from measurements with the University of Iowa Detector C on Pioneer 11. The phase space density was calculated assuming that the differential energy spectrum can be represented by a power law with index $\gamma = 1.3$. [From Van Allen, 1983].

Figure 2. Fits of a one-dimensional diffusion model (parabolic curve) and linear slope estimates (straight lines) to the Pioneer 11 inbound counting rates of Iowa Detector C. The cyclic variation of the counting rates is a result of spacecraft rotation. [From Van Allen, 1983].

Figure 3. Integral omnidirectional injection rates for CRAND protons versus radial distance calculated from Monte Carlo models for secondary neutron production by cosmic ray interactions in the main Saturnian rings. [From Cooper, 1983].

Figure 4. Omnidirectional fluxes of > 80 MeV CRAND protons as derived from counting rates by the University of Iowa Detector C and the University of California at San Diego M3 Detector on Pioneer 11.

Figure 5. Comparison of the Iowa Detector C fluxes with one-dimensional diffusion models for a series of assumed values of the mean particle lifetime $\tau$. In each case, the radial diffusion rate $D$ was determined by a minimum variance fit to the data profile. Note that the model profiles become imperceptibly different from the observed profiles for sufficiently large $\tau$-values.

Figure 6. RMS deviations of the model profiles of Figure 5 from the data profiles for each of the maxima centered on 2.43 and 2.67 $R_S$. These deviations asymptotically approach minima when the particle lifetime $\tau$ is increased to large values.

Figure 7. Voyager 2 'Enceladus' microsignature in low-energy ions and relativistic electrons. [From Carbary et al., 1983].

Figure 8. Voyager 2 LECP 'Mimas' microsignature at 3 ion energies for different pitch angles $\alpha$.

Figure 9. Mean stopping distances or ranges of electrons, protons, and singly ionized oxygen atoms in materials chosen as proxies for water ice. The right scale is the corresponding penetration distance for an assumed mass density of 1 gm/cm$^2$. [From Hood, 1989].

Figure 10. Integral intensities of electrons with $E_e > 0.040$ and $E_e > 0.56$ MeV as measured with the University of Iowa energetic particle instrument on Pioneer 11. [From Van Allen, 1984].

Figure 11. Similar to Figure 10 but showing a comparison between inbound and outbound integral intensities of electrons with $E_e > 0.040$ MeV. [From Van Allen, 1984].

Figure 12. Omnidirectional counting rates of energetic electrons in several energy ranges versus dipole $L$ as measured with the LECP instrument during the outbound trajectory of

Voyager 2. Note the increasing amplitudes of the counting rate minima centered on 4.0-4.5 $R_S$ with decreasing electron energy. [From Van Allen, 1984].

Figure 13. Ratio of the maximum directional flux of electrons with $E_e > 0.040$ MeV to that at a pitch angle of 89° versus radial distance. These ratios were derived from fits of Fourier cosine series to observed pitch angle distributions. Values greater than unity indicate a relative depletion of nearly equatorially mirroring electrons.

Figure 14. Comparison between the electron counting rate profiles of Figure 12 to model curves (dashed lines) calculated from a one-dimensional lossy diffusion model assuming no particle sources. The product $\tau D$ is the ratio of the electron lifetime to the time required for radial diffusion across a distance of $\sim 1$ $R_S$. The increasing depth of the observed minima with decreasing electron energy result in decreasing values of $\tau D$.

Figure 15. Summary of previous estimates for the diffusion rate of low energy (co-rotation dominated) ions and electrons in Saturn's magnetosphere. The symbols represent estimates based on observed energetic particle microsignatures of known satellites while the solid lines are functional forms of $D(L)$ that produced optimal fits to experimentally derived phase space density profiles. The curve labeled 'a' was for a model that assumed satellite absorption losses only; 'b' was for a model including nominal Ring E Absorption losses; 'c' assumed pitch angle scattering losses at a rate of one-tenth that of the strong pitch angle diffusion rate; and 'd' assumed strong pitch angle diffusion losses. Curve 'a' is unrealistically low due to the neglect of distributed losses. Curve 'd' is unrealistically high as evidenced by the disagreement with microsignature estimates. Thus the most probable range for $D$ near the E Ring maximum is $10^{-9}$ to $10^{-8}$ $R_S^2$ $s^{-1}$. [After Hood, 1985].

Figure 17. Radial dependence of the phase space density (in arbitrary units) of equatorially mirroring electrons with first invariant $\mu = 525$ MeV/G derived from counting rates by Detectors A and B of the University of Iowa instrument on Pioneer 11. In order to calculate this profile, a power law energy spectrum with index $\gamma = 3.8$ was assumed with a low energy cut-off at an energy corresponding to the first invariant value.

Figure 18. Comparison between the phase space density profile of Figure 17 and model profiles calculated for a series of assumed loss models. Note that as increasingly lossy absorption models are assumed, the satellite absorption dips are smoothed out resulting in improved agreement with the data profile.

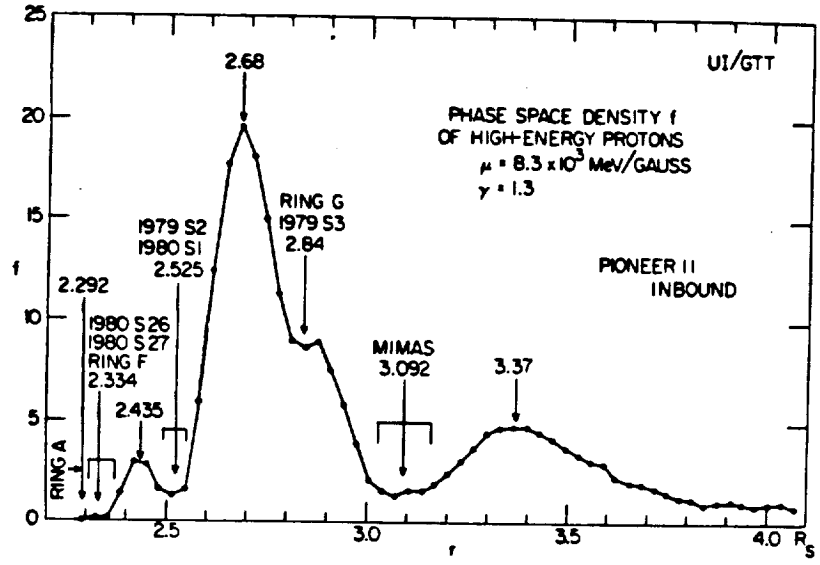


Figure 1. Radial dependence of phase space density (in arbitrary units) of equatorially mirroring CRAND protons derived from measurements with the University of Iowa Detector C on Pioneer 11. The phase space density was calculated assuming that the differential energy spectrum can be represented by a power law with index $\gamma = 1.3$. [From Van Allen, 1983].

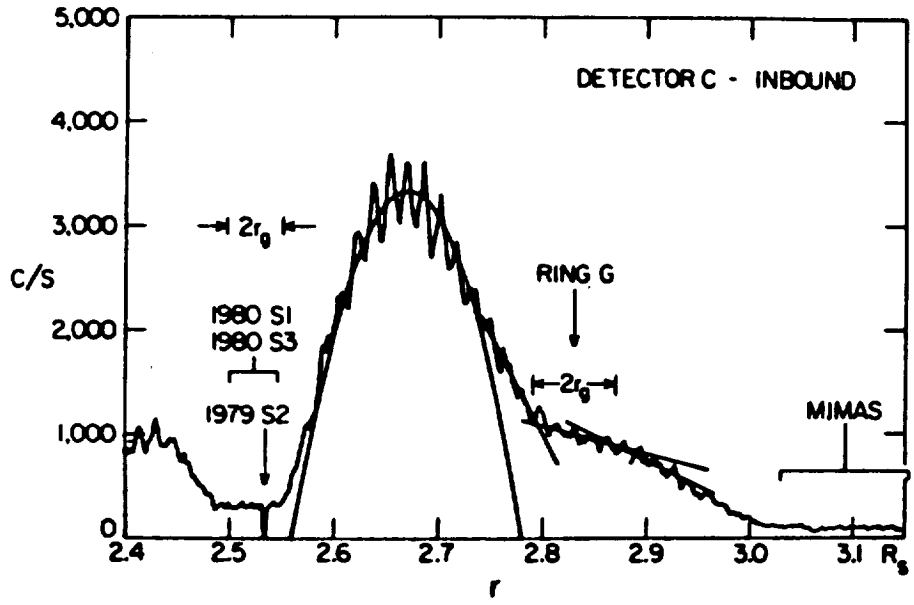


Figure 2. Fits of a one-dimensional diffusion model (parabolic curve) and linear slope estimates (straight lines) to the Pioneer 11 inbound counting rates of Iowa Detector C. The cyclic variation of the counting rates is a result of spacecraft rotation. [From Van Allen, 1983].

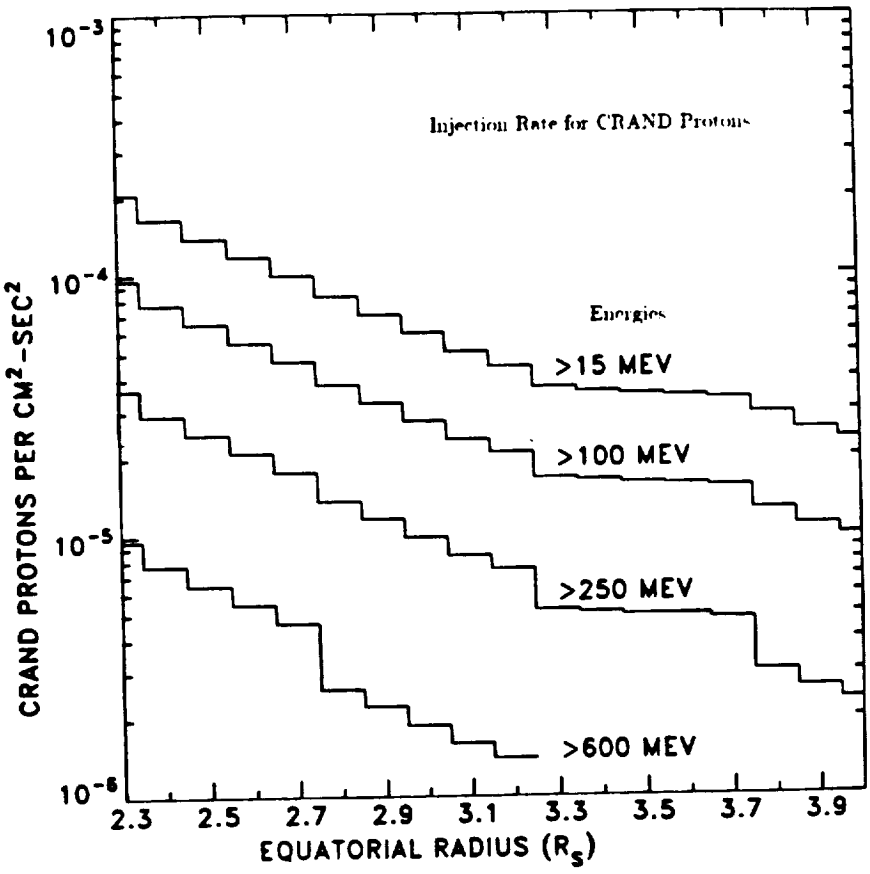


Figure 3. Integral omnidirectional injection rates for CRAND protons versus radial distance calculated from Monte Carlo models for secondary neutron production by cosmic ray interactions in the main Saturnian rings. [From Cooper, 1983].

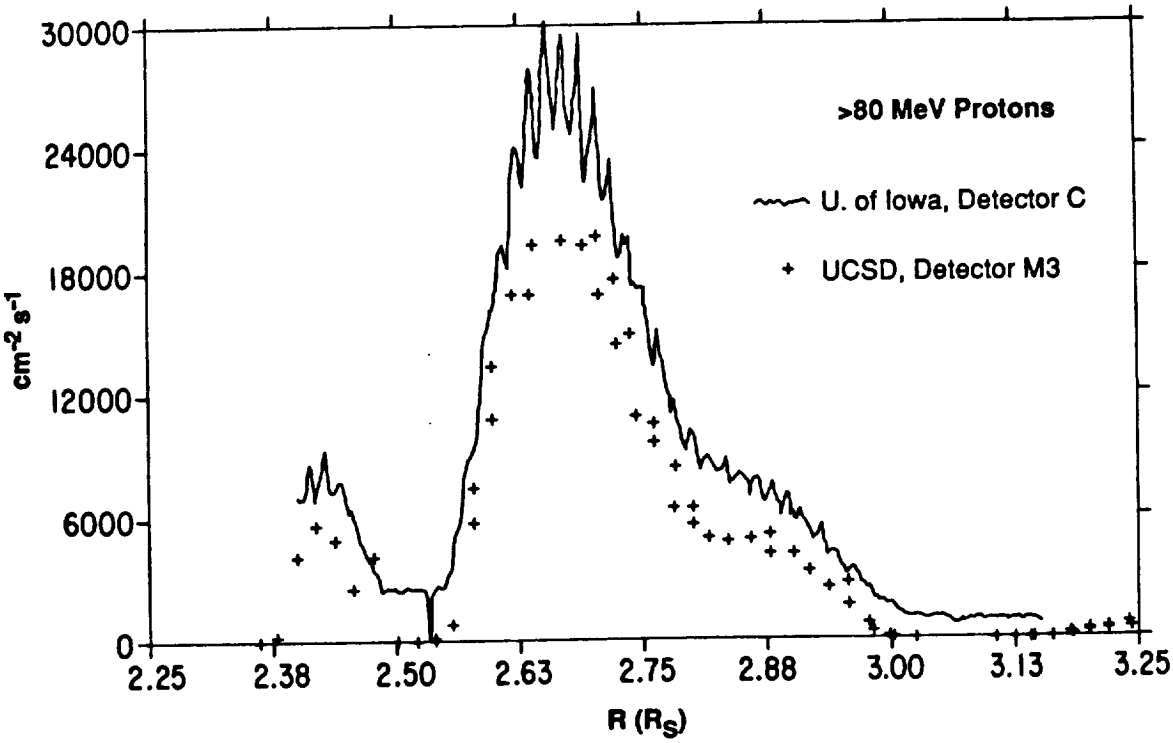


Figure 4. Omnidirectional fluxes of > 80 MeV CRAND protons as derived from counting rates by the University of Iowa Detector C and the University of California at San Diego M3 Detector on Pioneer 11.

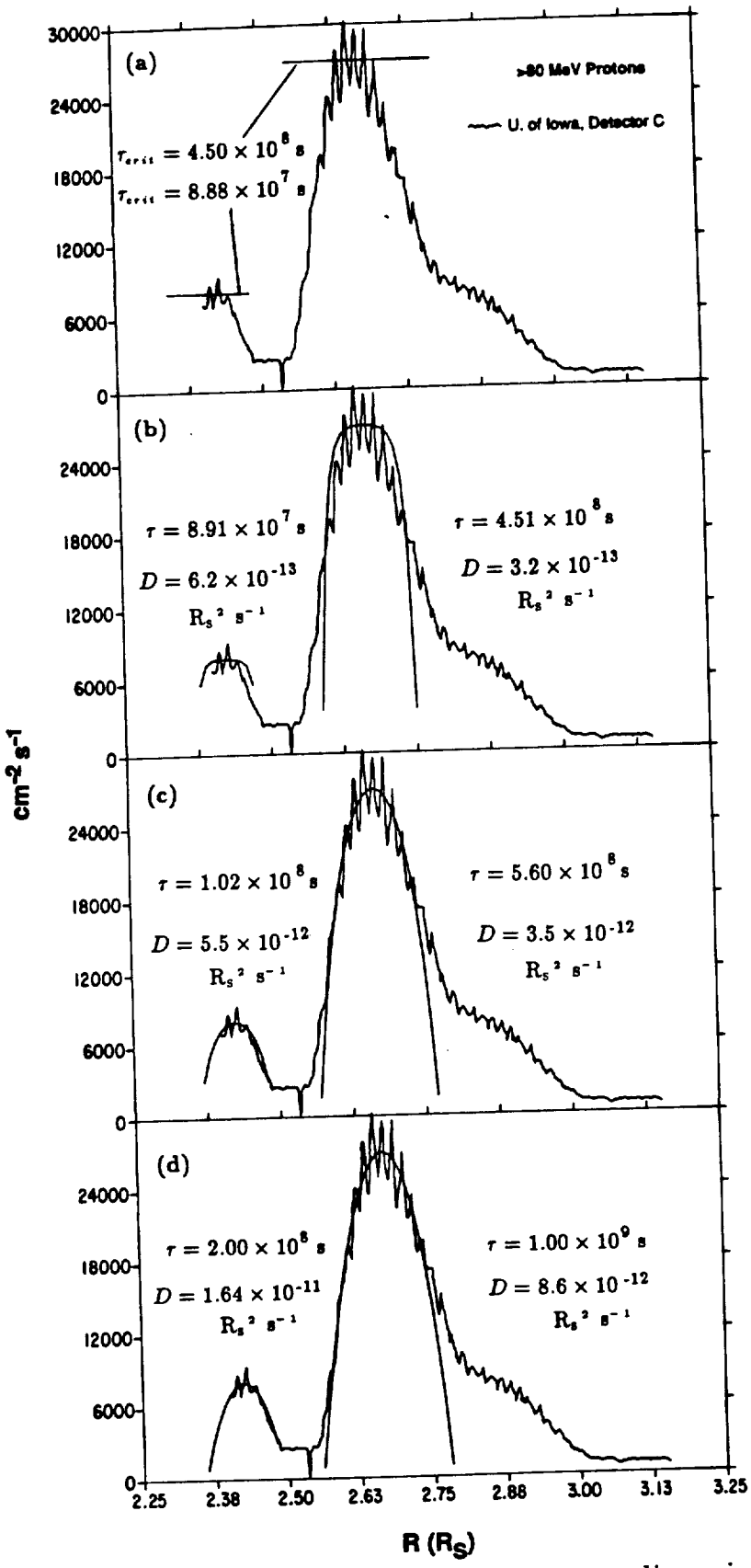


Figure 5. Comparison of the Iowa Detector C fluxes with one-dimensional diffusion models for a series of assumed values of the mean particle lifetime $\tau$. In each case, the radial diffusion rate $D$ was determined by a minimum variance fit to the data profile. Note that the model profiles become imperceptibly different from the observed profiles for sufficiently large $\tau$-values.

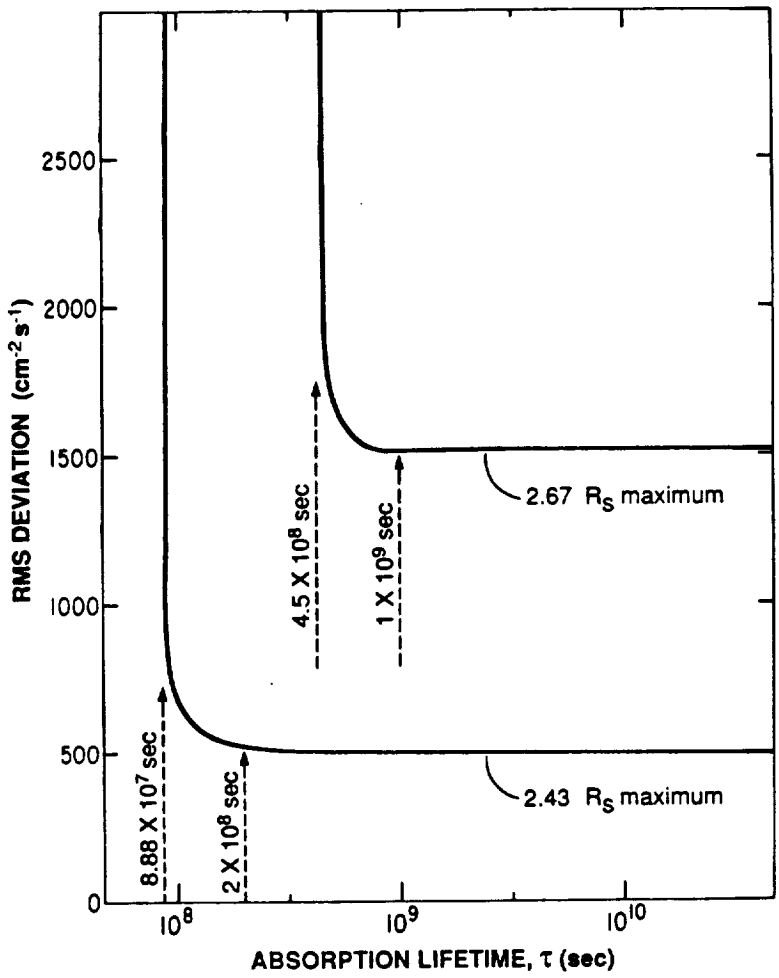


Figure 6. RMS deviations of the model profiles of Figure 5 from the data profiles for each of the maxima centered on 2.43 and 2.67 $R_S$. These deviations asymptotically approach minima when the particle lifetime $\tau$ is increased to large values.

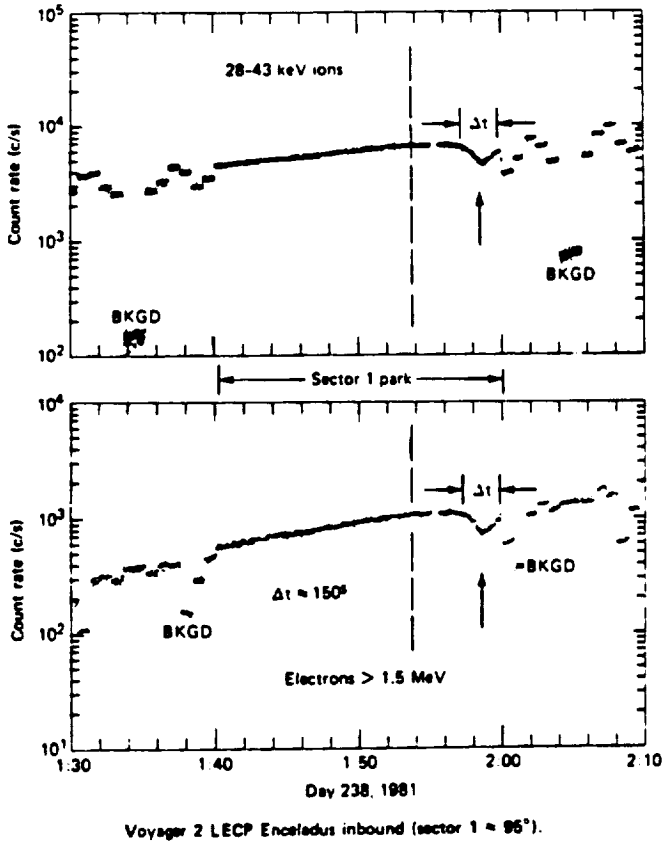


Figure 7. Voyager 2 'Enceladus' microsignature in low-energy ions and relativistic electrons. [From Carbary et al., 1983].

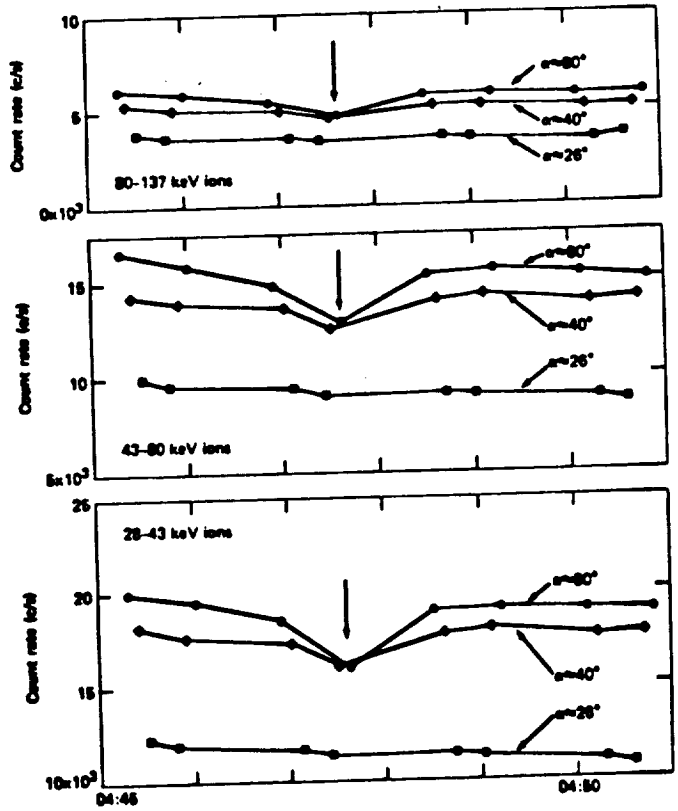




Figure 8. Voyager 2 LECP 'Mimas' microsignature at 3 ion energies for different pitch angles $\alpha$.

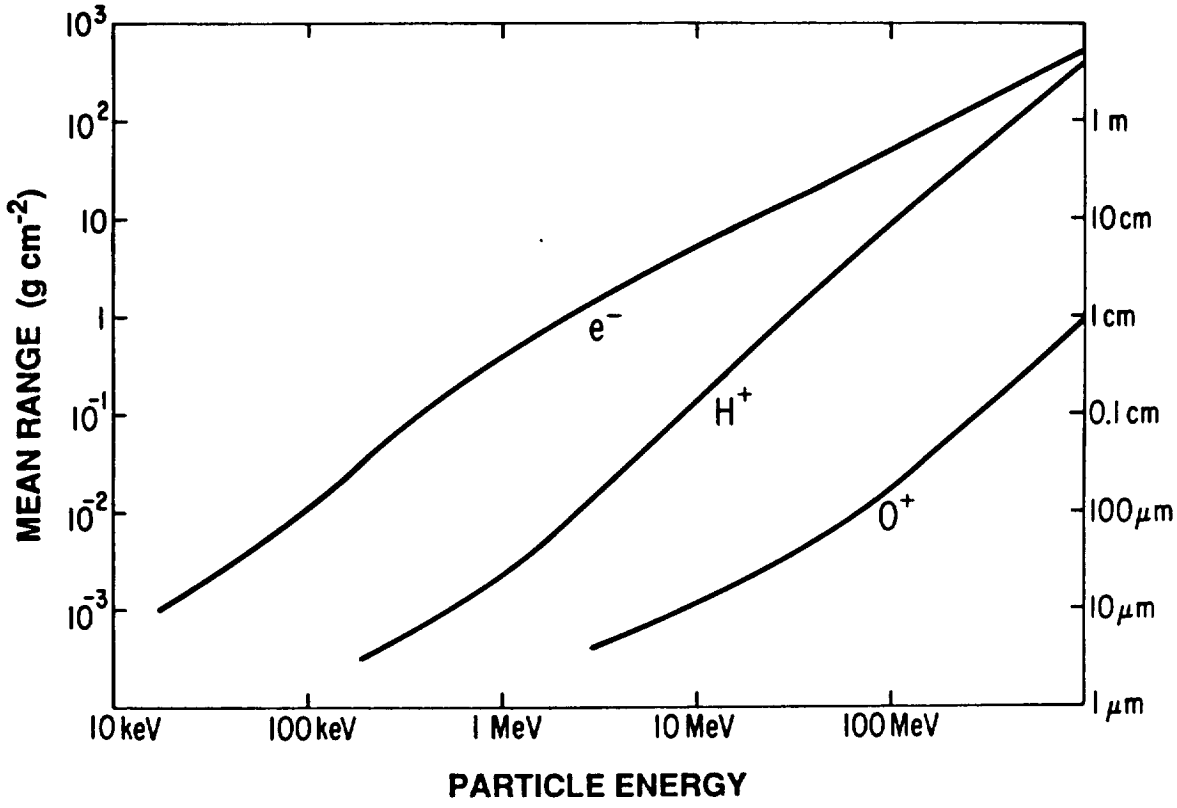


Figure 9. Mean stopping distances or ranges of electrons, protons, and singly ionized oxygen atoms in materials chosen as proxies for water ice. The right scale is the corresponding penetration distance for an assumed mass density of 1 gm/cm$^2$. [From Hood, 1989].

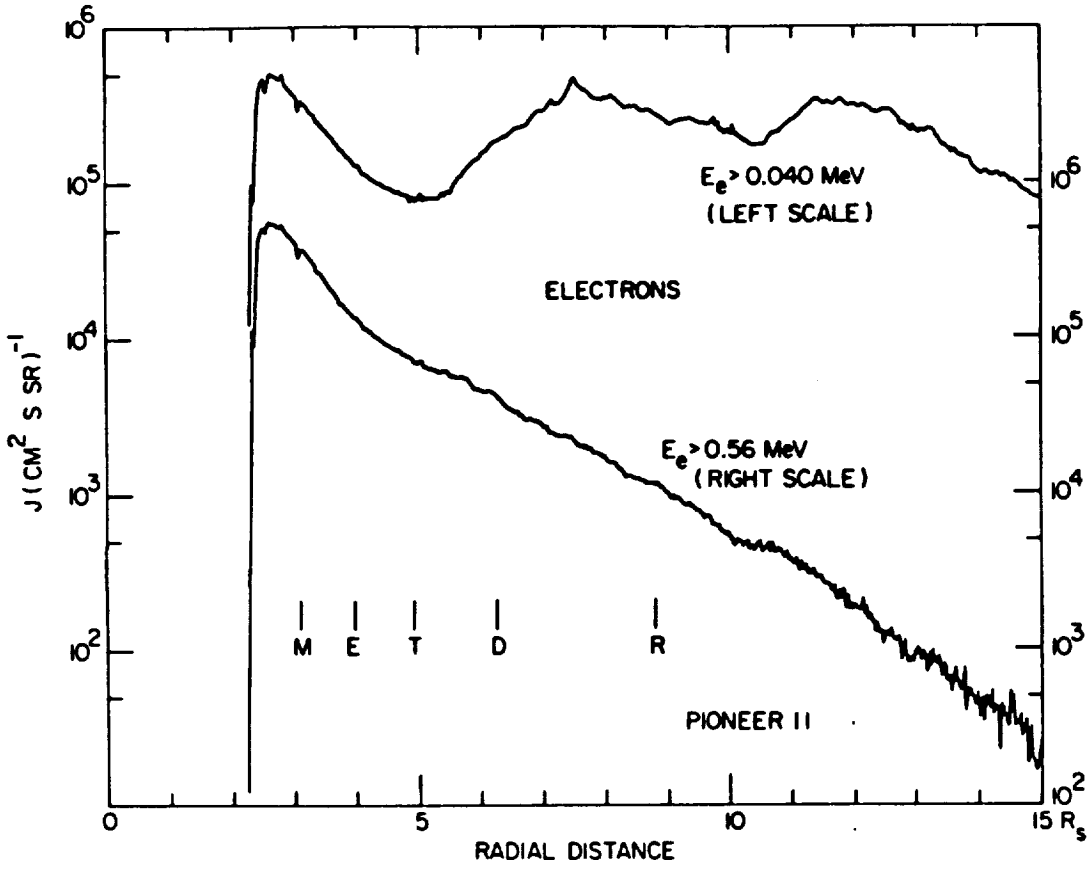


Figure 10. Integral intensities of electrons with $E_e > 0.040$ and $E_e > 0.56$ MeV as measured with the University of Iowa energetic particle instrument on Pioneer 11. [From Van Allen, 1984].

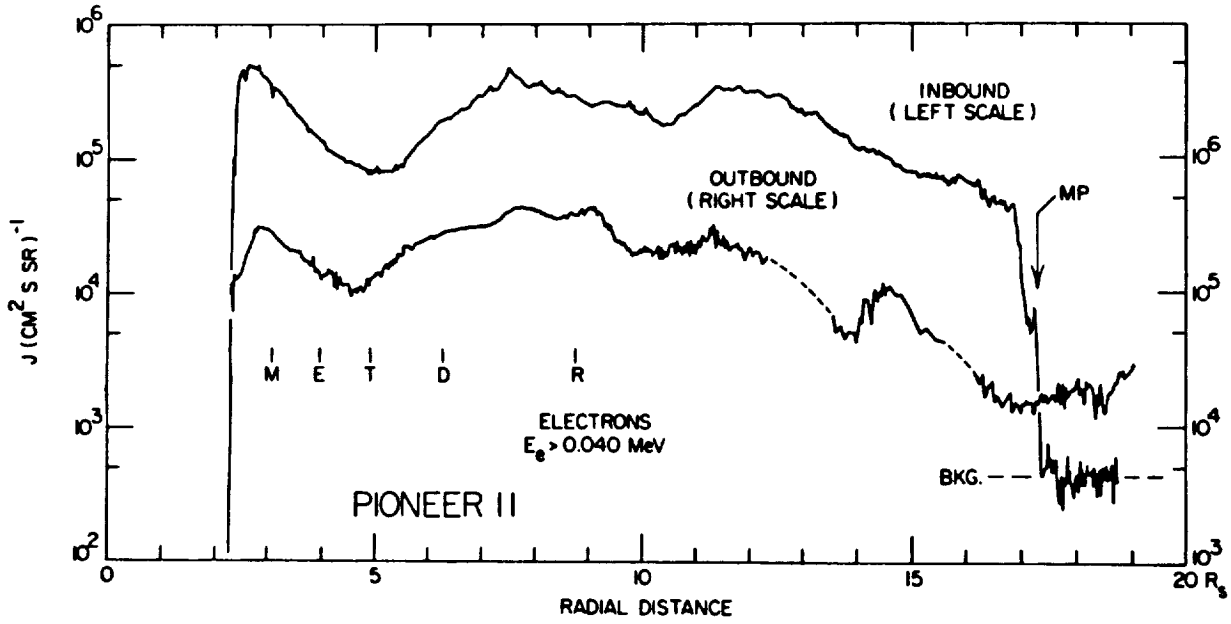


Figure 11. Similar to Figure 10 but showing a comparison between inbound and outbound integral intensities of electrons with $E_e > 0.040$ MeV. [From Van Allen, 1984].

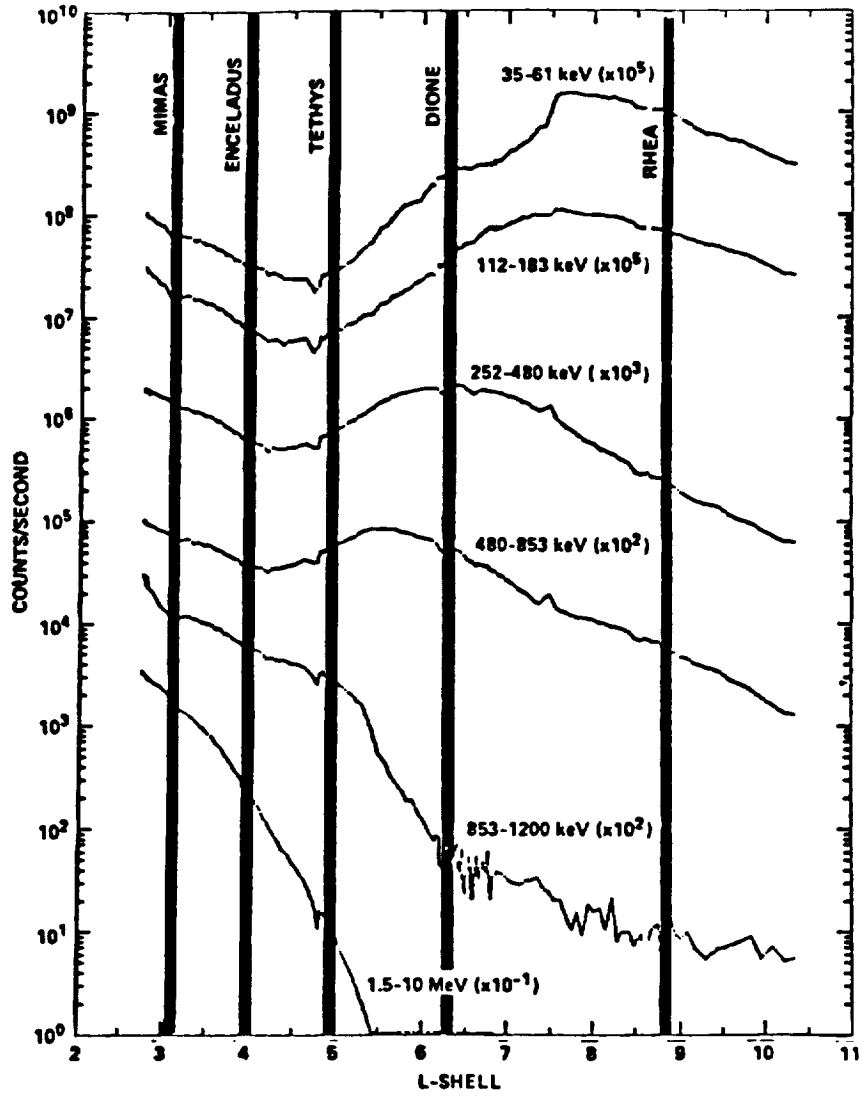


Figure 12. Omnidirectional counting rates of energetic electrons in several energy ranges versus dipole $L$ as measured with the LECP instrument during the outbound trajectory of Voyager 2. Note the increasing amplitudes of the counting rate minima centered on 4.0-4.5 $R_S$ with decreasing electron energy. [From Van Allen, 1984].

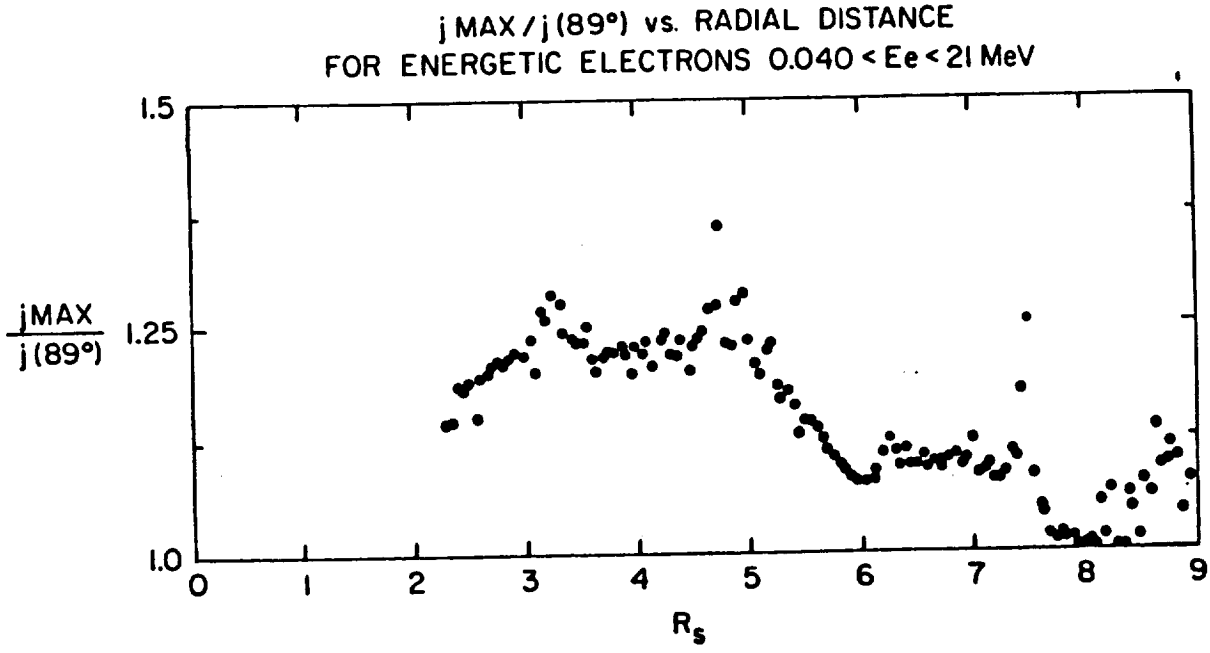


Figure 13. Ratio of the maximum directional flux of electrons with $E_e > 0.040$ MeV to that at a pitch angle of 89° versus radial distance. These ratios were derived from fits of Fourier cosine series to observed pitch angle distributions. Values greater than unity indicate a relative depletion of nearly equatorially mirroring electrons.

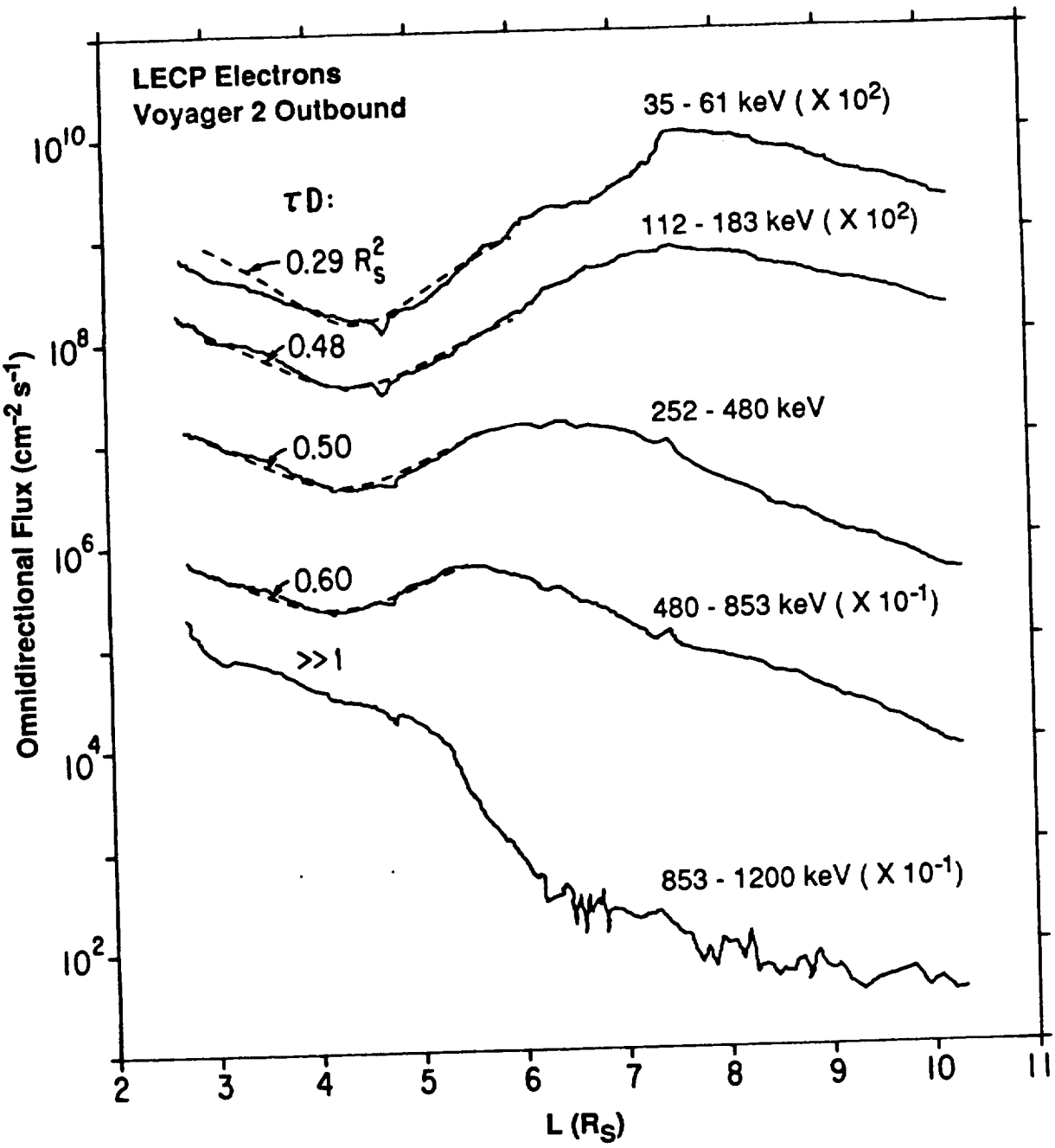


Figure 14. Comparison between the electron counting rate profiles of Figure 12 to model curves (dashed lines) calculated from a one-dimensional lossy diffusion model assuming no particle sources. The product $\tau D$ is the ratio of the electron lifetime to the time required for radial diffusion across a distance of $\sim$ 1 $R_S$. The increasing depth of the observed minima with decreasing electron energy result in decreasing values of $\tau D$.

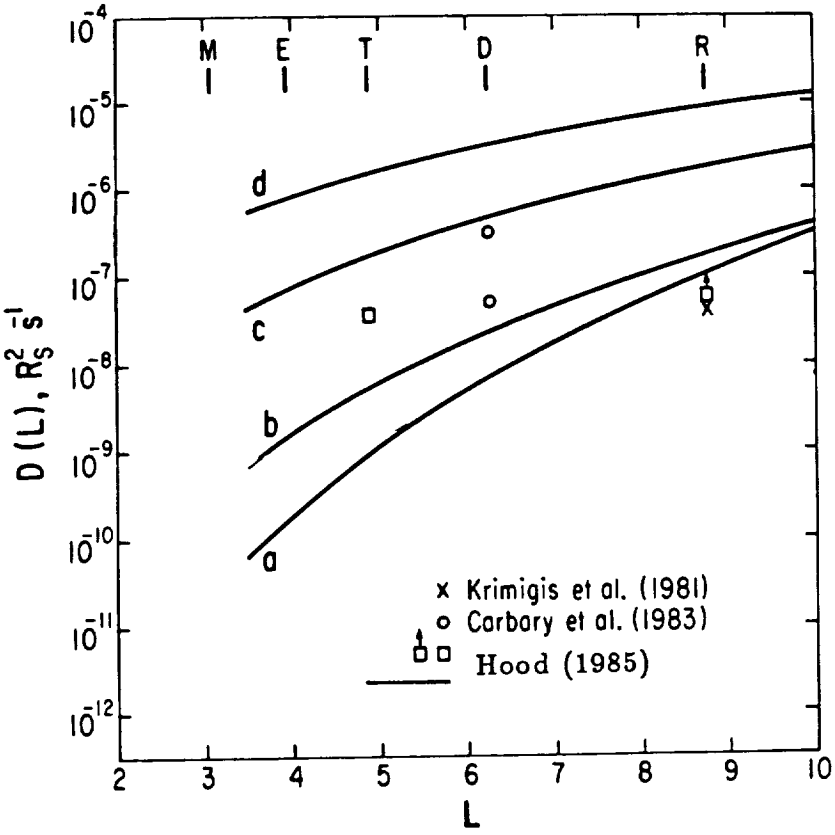


Figure 15. Summary of previous estimates for the diffusion rate of low energy (co-rotation dominated) ions and electrons in Saturn's magnetosphere. The symbols represent estimates based on observed energetic particle microsignatures of known satellites while the solid lines are functional forms of $D(L)$ that produced optimal fits to experimentally derived phase space density profiles. The curve labeled 'a' was for a model that assumed satellite absorption losses only; 'b' was for a model including nominal Ring E Absorption losses; 'c' assumed pitch angle scattering losses at a rate of one-tenth that of the strong pitch angle diffusion rate; and 'd' assumed strong pitch angle diffusion losses. Curve 'a' is unrealistically low due to the neglect of distributed losses. Curve 'd' is unrealistically high as evidenced by the disagreement with microsignature estimates. Thus the most probable range for $D$ near the E Ring maximum is $10^{-9}$ to $10^{-8}$ $R_S^2$ $s^{-1}$. [After Hood, 1985].

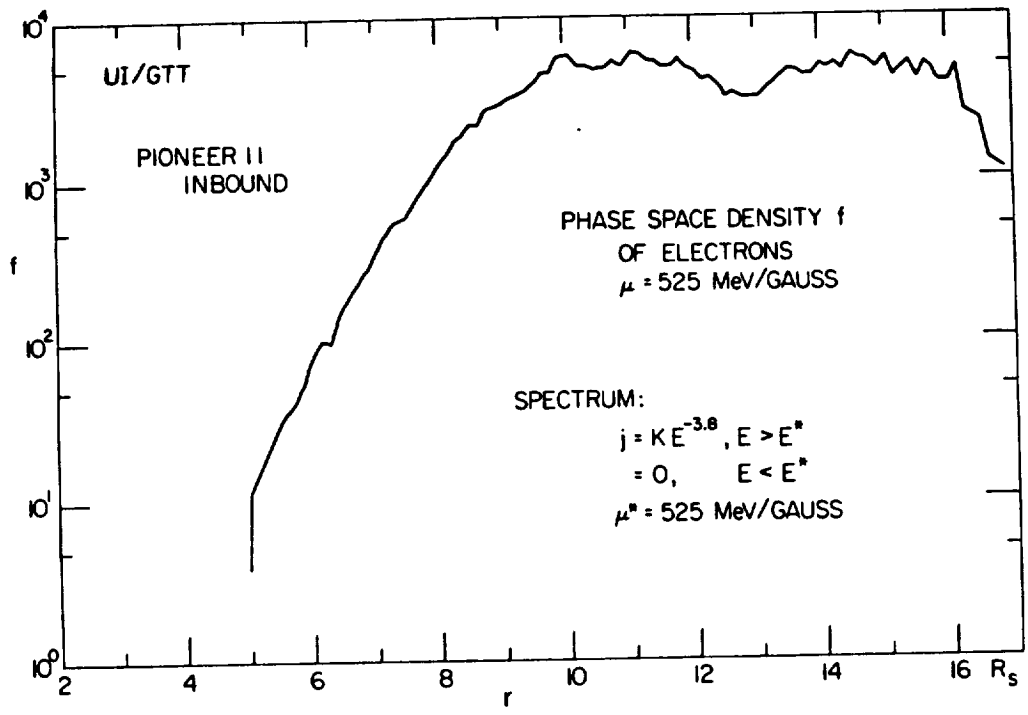


Figure 16. Radial dependence of the phase space density (in arbitrary units) of equatorially mirroring electrons with first invariant $\mu = 525$ MeV/G derived from counting rates by Detectors A and B of the University of Iowa instrument on Pioneer 11. In order to calculate this profile, a power law energy spectrum with index $\gamma = 3.8$ was assumed with a low energy cut-off at an energy corresponding to the first invariant value. [From Van Allen, 1984].

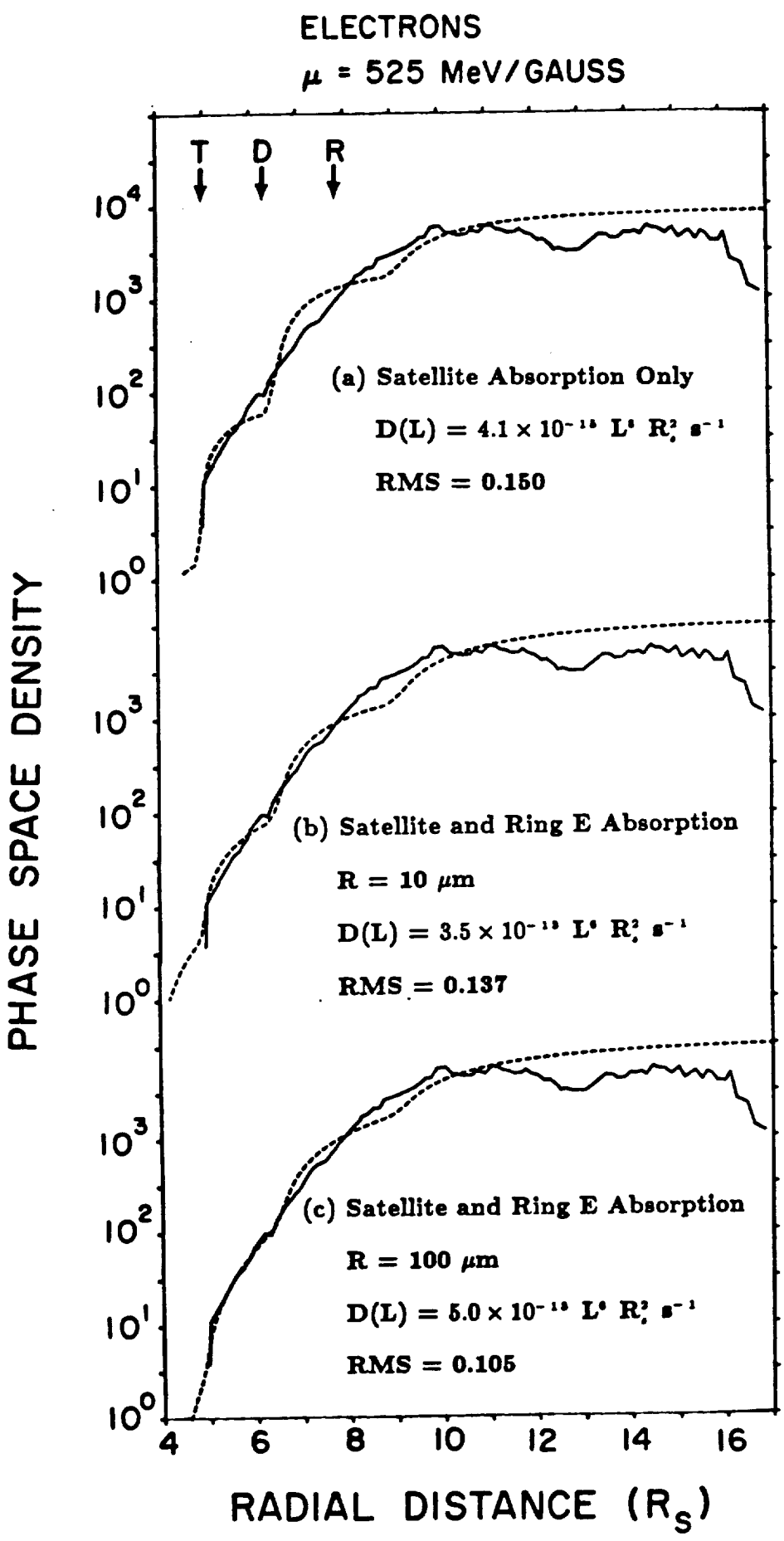


Figure 17. Comparison between the phase space density profile of Figure 17 and model profiles calculated for a series of assumed loss models. Note that as increasingly lossy absorption models are assumed, the satellite absorption dips are smoothed out resulting in improved agreement with the data profile.

## Publications Resulting from this Contract

Cuzzi, J. N., J. F. Cooper, L. L. Hood, and M. R. Showalter, Abundance and size distribution of ring material outside of the main rings of Saturn, Report of the Cassini Dust Environment Workshop, submitted to the Cassini Project, May, 1989.

Hood, L. L., Constraints on the Physical Properties of Saturn's G and E rings from Energetic Charged Particle Measurements, *J. Geophys. Res.*, submitted, July, 1990.